*Journal of Advanced Ceramics*
2020, **9**(3): 320–328
https://doi.org/10.1007/s40145-020-0371-z
ISSN 2226-4108
CN 10-1154/TQ

**Research Article**

# Single-source-precursor synthesis and phase evolution of SiC–TaC–C ceramic nanocomposites containing core–shell structured TaC@C nanoparticles

Zhaoju YU[a,b,*], Yujing YANG[a], Kangwei MAO[a], Yao FENG[c], Qingbo WEN[c,*], Ralf RIEDEL[c]

[a]*College of Materials*, *Key Laboratory of High Performance Ceramic Fibers* (*Xiamen University*), *Ministry of Education*, *Xiamen 361005*, *China*
[b]*College of Materials*, *Fujian Key Laboratory of Advanced Materials*, *Xiamen University*, *Xiamen 361005*, *China*
[c]*Technische Universität Darmstadt*, *Institut für Materialwissenschaft*, *Darmstadt 64287*, *Germany*

Received: January 6, 2020; Revised: February 17, 2020; Accepted: February 27, 2020


**Abstract:** A novel single-source-precursor for SiC–TaC–C nanocomposites was successfully synthesized by the chemical reaction between a polycarbosilane (allylhydridopolycarbosilane, AHPCS) and tantalum(V) chloride ($TaCl_5$), which was confirmed by Fourier transform infrared spectra (FTIR) measurement. After pyrolysis of the resultant single-source-precursors at 900 ℃, amorphous ceramic powders were obtained. The 900 ℃ ceramics were annealed at different temperatures in the range of 1200–1600 ℃ to gain SiC–TaC–C nanocomposites. The phase evolution of ceramic nanocomposites was investigated by X-ray diffraction (XRD) and transmission electron microscopy (TEM). The results indicate that the TaC starts to crystallize at lower temperature than the β-SiC. It is particularly worth pointing out that the unique core–shell structured TaC@C nanoparticles were *in-situ* formed and homogeneously distributed in the ceramic matrix after annealing at 1400 ℃. Even at a high temperature of 1600 ℃, the grain sizes of β-SiC and TaC are smaller than 30 nm, fulfilling the definition of nanocomposites. The present study related to SiC–TaC–C nanocomposites paves a new road for enriching ultra-high temperature ceramic family suitable for structural/functional applications in harsh environment.

**Keywords:** polymer-derived ceramics; TaC; SiC; nanocomposites; core–shell structure

## 1 Introduction

As well known, ultra-high temperature ceramics (UHTCs) usually have to fulfill the requirement with high melting points beyond 3000 ℃ (sometimes 3000 K). Within this context, borides, carbides, and nitrides of group 4 transition metals are considered to be typical UHTCs [1–5]. Tantalum carbide (TaC) exhibits many unique properties, such as extremely high melting point (3880 ℃), high hardness (20 GPa), high elastic modulus (560 GPa), high density (14.6 g/cm$^3$), and good chemical stability, which is considered as one of the most important UHTC family members [1–10]. These properties make TaC a suitable candidate for

* Corresponding authors.
E-mail: Z. Yu, zhaojuyu@xmu.edu.cn;
Q. Wen, wentsingbo@materials.tu-darmstadt.de

high-temperature applications in the fields of aerospace, metallurgy, and machinery [11]. For example, it has broad application prospects in rocket nozzles, scramjet propulsion, brake discs, high-performance cutting tools, cold punch dies, and aerospace propulsion systems [12–17]. However, the poor fracture toughness and weak sintering properties impair the applications of bulk material in harsh environment [18–20]. In addition, similar to other related UHTC systems, TaC suffers from rather poor oxidation resistance at high temperatures [21].

An effective way to solve the above-mentioned problem is to form composites by introducing a second phase to TaC [22]. It has been reported that the addition of SiC, $TaSi_2$, $TaB_2$, or $MoSi_2$ promotes densification and decreases the grain growth of TaC [23–26]. For example, TaC–SiC ceramic composites have better mechanical strength than individual TaC ceramics, and the addition of SiC can improve the oxidation resistance and ablation resistance of the ceramics [6,27–29]. Recently, SiC–UHTC nanocomposites have attracted numerous attention since by reducing the size of components within the composites towards the nanoscale, an enormous improvement in their properties (e.g., mechanical, electrical, electromagnetic, oxidation resistance, and ablation resistance) can be achieved [30–43]. Polymer derived ceramics (PDCs) are synthesized via solid-state thermolysis of preceramic polymers and exhibit a unique combination of remarkable properties and tailorable microstructure [33]. The PDC approach is effective to fabricate this kind of SiC–UHTC nanocomposite family [1,34,35,44–48]. For example, ZrC–$ZrB_2$–SiC ceramic nanocomposites were effectively prepared by a single-source-precursor route, with allylhydridopolycarbosilane (AHPCS), triethylamine borane, and bis(cyclopentadienyl)zirconium dichloride as starting materials [48].

In our previous study, we successfully synthesized Hf-based UHTCs/SiC/C ceramic nanocomposites with a core–shell structure, which was confirmed that the $HfC_xN_{1-x}$, $Hf_yTa_{1-y}C_xN_{1-x}$-based UHTC phase serves as core and amorphous carbon as shell [34,38,41,43]. The carbon shell acts as a diffusion barrier to suppress grain growth of $HfC_xN_{1-x}$ and $Hf_yTa_{1-y}C_xN_{1-x}$ at high temperatures, which is advantageous for high-temperature properties [34]. Moreover, the thickness of carbon shell can be controlled by the molecular tailoring of the preceramic precursor, which plays an important role on tuning the electrical conductivity of the resultant nanocomposites [41]. The unique core–shell structure endows the resultant UHTCs/SiC/C nanocomposites not only high-temperature resistance but also advanced functional properties towards electromagnetic applications [38,43]. However, a small amount of nitrogen is always unavoidable since we used N-containing Hf and/or Ta compounds (such as pentakis(dimethylamino)tantalum(V), tetrakis(dimethylamido)hafnium(IV), tetrakis(diethylamino)hafnium(IV)) as UHTC sources [34,38,41,43]. The existence of N leads to decomposition and obvious weight loss at 1500 ℃ [34]. In the present study, we replaced N-containing Hf and Ta compounds as $TaCl_5$ to form a single-source-precursor for TaC–SiC–C ceramic nanocomposites via PDC approach. Finally, the core–shell structured TaC@C nanoparticles were *in-situ* formed and homogeneously distributed in the SiC matrix. The resultant TaC–SiC–C nanocomposites are promising for combined structural and functional materials applied in harsh environments.

## 2 Experimental

### 2.1 Materials

$TaCl_5$ with a 95% purity was provided by Aladdin (Shanghai, China). The AHPCS with formula $[SiH_{1.30}(CH_3)_{0.60}(CH_2CH{=}CH_2)_{0.10}CH_2]_n$ was prepared according to our previous study [49]. Chloroform ($CHCl_3$) was distilled before use. All synthetic operations were carried out in the high vacuum or inert environment described by Shriver and Drezdzon [50]. The Ar atmosphere with purity of 99.99% was used for pyrolysis process. Other commercially available chemicals were also used as received.

### 2.2 Precursor synthesis

Firstly, white $TaCl_5$ powders were introduced into a 250 mL Schlenk flask in Ar, and subsequently 60 mL $CHCl_3$ was added into the flask to dissolve $TaCl_5$ until a clear solution was obtained. Then, AHPCS was introduced into the mixture at 25 ℃ and the obtained mixture was heated up to 60 ℃ for 1 h. After the solvent $CHCl_3$ was removed under vacuum, the resultant viscous yellow solution was heated up to 160 ℃ for 6 h. Finally, the synthesized single-source-precursors with different weight ratios of $TaCl_5$/AHPCS 1/2, 1/10, and 1/30 are denoted as PTA-1,

PTA-2, and PTA-3, respectively. To make a comparison, AHPCS was heat treated at the same conditions (160 ℃ for 6 h), and the resultant polymer was named as blank-AHPCS.

### 2. 3 Polymer-to-ceramic transformation

The pyrolysis and annealing procedure were performed in tube furnaces under the Ar atmosphere. Briefly, the single-source-precursors were pyrolyzed at 900 ℃ to obtain amorphous ceramic powders. The 900 ℃ ceramics were annealed at different temperatures in the range of 1200–1600 ℃. The synthesis process from single-source-precursors to ceramic powders and heating program are shown in Fig. 1.

### 2. 4 Characterization

Fourier transform infrared spectra (FTIR, Nicolet, Madison, WI, USA) was measured with the Nicolet Avator 360 apparatus to analyze the molecular structure of single-source-precursors. Powder X-ray diffraction (XRD) experiments were recorded using a STADI P powder diffractometer (STOE & Cie GmbH, Darmstadt, Germany) with molybdenum $K\alpha_1$ radiation source. The weight fractions of crystallized phases including TaC and SiC annealed at 1600 ℃ are determined by Rietveld refinement of the XRD patterns of the ceramics with the FullProf software [51]. The thermal properties of cured precursors annealed at 300 ℃ were performed by TGA (SHIMADZU, DTG- 60H, Japan) in Ar gas with a heating rate of 10 ℃/min ranging from room temperature to 1000 ℃. IRIS intrepid inductively coupled plasma mass spectrometry (ICP-MS, Thermo Electron Corporation, America) was used to measure the contents of Ta. Elemental analysis of the samples was examined by Horiba oxygen/nitrogen analyzer EMGA-620 W for oxygen element, Horiba carbon/sulfur analyzer EMIA-320 V (Horiba, Kyoto, Japan) for carbon element, and elemental analyzer EA/MA1110 (Carlo Erba, Italy) for hydrogen element. The microstructure of ceramic samples was observed by transmission electron microscope (TEM, JEM-2100, JEOL, Tokyo, Japan) at an acceleration voltage of 200 kV.

## 3 Results and discussion

### 3. 1 Precursor characterization

To trace the structural evolution during precursor synthesis, Fig. 2(a) shows the FTIR spectra of original AHPCS, the unreacted AHPCS/$TaCl_5$ mixture, blank-AHPCS as well as the obtained single-source-precursors. Moreover, the single-source-precursor PTA-1, PTA-2, and PTA-3 were synthesized with different weight ratios of $TaCl_5$/AHPCS 1/2, 1/10, and 1/30 in the feed, respectively.

According to the previous study, the main typical absorption peaks of AHPCS are marked and shown in Fig. 2(a) [49]. Compared with the original AHPCS, the absorption band of C=C–H at 3077 $cm^{-1}$ almost disappears for the blank-AHPCS and single-source-precursors PTA-1, PTA-2, and PTA-3 (Fig. 2(b)), indicating that the hydrosilylation (C=C/Si–H) occurred to consume C=C bonds with and without introduction of $TaCl_5$. It is particularly worth mentioning that the intensities of Si–H stretch absorption band at 2140 $cm^{-1}$ significantly reduce with increasing $TaCl_5$ content in the feed. Based on Ref. [52] that the $Cp_2MCl_2$ (M= Ti,Zr,Hf) can be incorporated into the polycarbosilane chains by HCl elimination namely dehydrochlorication (Si–H/$Cp_2MCl_2$), in the present study, it is assumed that $TaCl_5$ is introduced into the AHPCS chains by dehydrochlorication (Si–H/$TaCl_5$) to consume Si–H groups.

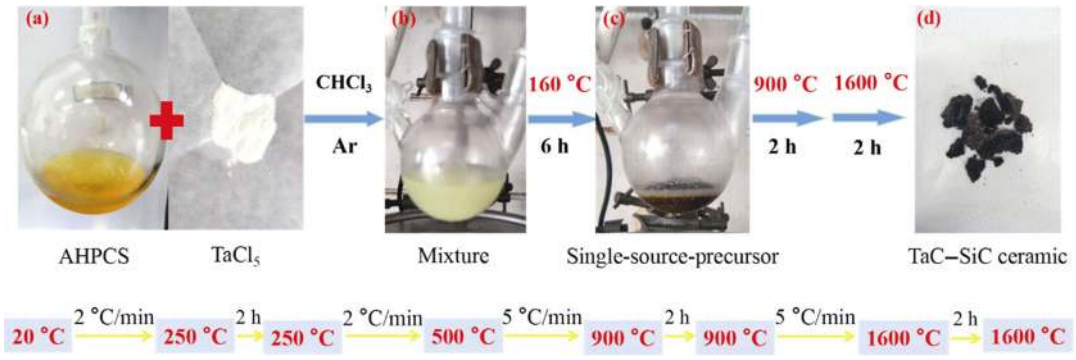


**Fig. 1** Photographic description of the synthesis process and heating program.

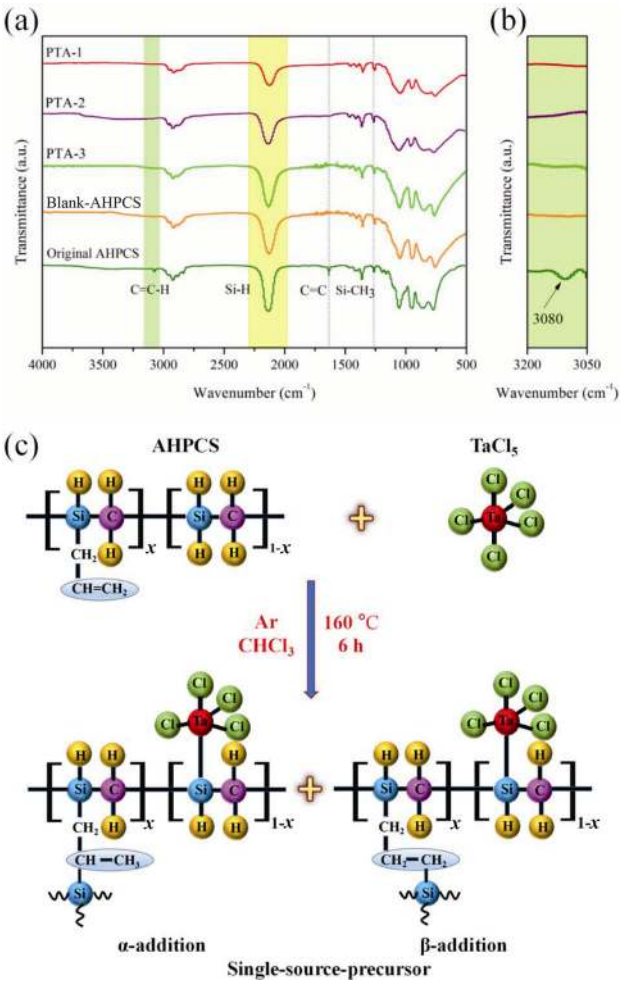


**Fig. 2** (a) FTIR spectra of original AHPCS, blank-AHPCS, and single-source-precursors and (b) the region from 3050 to 3200 $cm^{-1}$ is shown magnified. (c) Reaction pathways during the precursor synthesis.

According to the FTIR results, the reaction paths of the single-source-precursor PTA are demonstrated in Fig. 2(c): 1) the dehydrochlorication between Ta–Cl and Si–H bonds is used to form single-source-precursors; 2) the hydrosilylation (C=C/Si–H) occurs to increase cross-linking of the obtained precursors.

The thermal behavior of single-source-precursors were performed by TGA and the results are shown in Fig. 3. The weight loss of blank-AHPCS starts at 300 ℃, due to the evolved $H_2$ from the dehydrocoupling (Si–H/Si–H) [33]. However, the weight loss of single-source-precursors occurs at the beginning (room temperature), indicating that the dehydrochlorication (Si–H/$TaCl_5$) continues during heat treatment. As a result, the evolution of HCl gas from the dehydrochlorication should be responsible for the weight loss at such low temperatures. In the range of

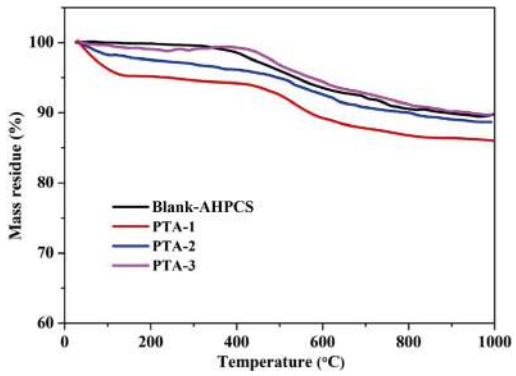


**Fig. 3** TGA curves of blank-AHPCS and single-source-precursors.

300–900 ℃, the precursors undergo main weight loss. From 900 to 1000 ℃, nearly no weight loss is observed, indicating the complete polymer-to-ceramic transformation. The ceramic yields at 1000 ℃ are 89.4 wt%, 89.4 wt%, 88.7 wt%, and 85.9 wt% for the blank-AHPCS, PTA-3, PTA-2, and PTA-1, respectively. With increasing $TaCl_5$ amounts in the feed, the ceramic yields slightly reduce, probably due to further occurrence of the dehydrochlorication for single-source-precursors at the early stage with the temperature below 300 ℃. In general, all the single-source-precursors exhibit very high ceramic yield (> 85 wt%).

### 3.2 Microstructure and phase evolution of ceramics

The phase compositions of ceramics were investigated by XRD and the results are shown in Fig. 4. Taking the PTA-2-derived ceramics as examples, Fig. 4(a) shows the phase evolution with increasing the annealing temperatures. The 900 ℃ ceramic is amorphous. At 1200 ℃, crystallization diffraction peaks start to appear despite that they are weak. However, it is difficult to distinguish the assignments of TaC and β-SiC since the diffraction peaks are broad, which will be further investigated by TEM. At 1400 ℃, the diffraction peaks of β-SiC (PDF 75-0254) appear and are mainly displayed at $2\theta$ = 16.1° (111), 26.6° (220), and 31.2° (311). Besides, the peaks at $2\theta$ = 15.8° (111), 18.2° (200), 26.0° (220), and 30.6° (311) attributed to the characteristics of TaC (PDF 35-0801). The results indicate that the SiC–TaC composites are formed. Further annealing at 1600 ℃ leads to the sharpening of characteristic peaks of β-SiC and TaC, suggesting the enhanced crystallization degree.

To investigate the influence of $TaCl_5$ content on the phase composition of resultant ceramics, XRD patterns

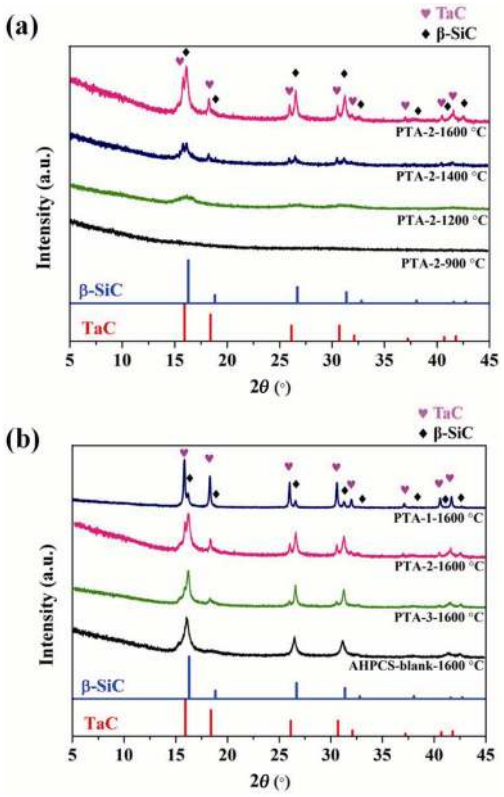


**Fig. 4** XRD patterns of (a) PTA-2-derived ceramics annealed at different temperatures and (b) blank-AHPCS, PTA-1, PTA-2, and PTA-3-derived ceramics annealed at 1600 ℃.

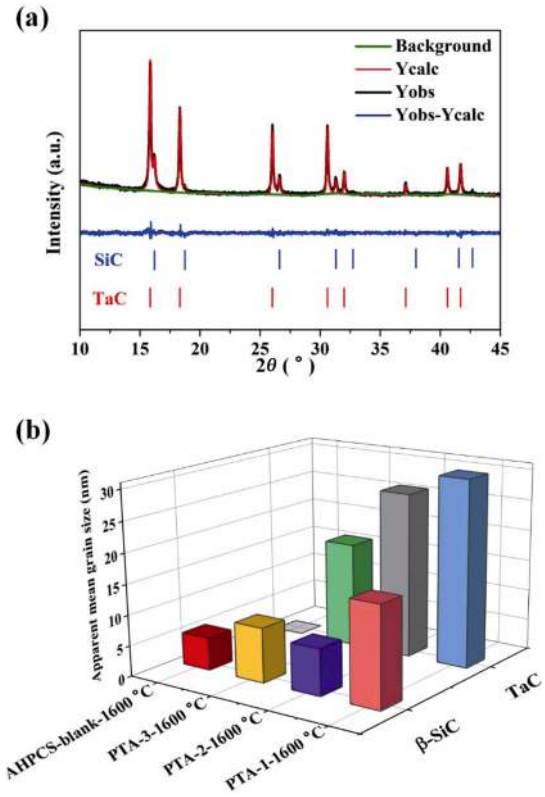


**Fig. 5** (a) Diffraction patterns of the ceramics annealed at 1600 ℃ with the result of Rietveld refinement. Yobs and Ycalc represent the observed and calculated profiles, respectively; the green line represents the background; the blue line at the bottom denotes the intensity difference between the observed and calculated profiles. (b) Estimated grain size of β-SiC and TaC by Rietveld refinement.

of different precursors derived ceramics annealed at 1600 ℃ were measured and compared in Fig. 5(b). The crystalline phases of TaC and β-SiC can be observed obviously in the three PTA-derived samples. As expected, the intensities of diffraction peaks from TaC increase with the increasing of $TaCl_5$ amount, indicating that the phase composition can be easily tuned by adjusting the $TaCl_5$ amount in the feed for precursor synthesis. A Rietveld refinement of the powder pattern of the 1600 ℃ ceramics was performed using the FullProf software, and the results are shown in Fig. 5(a). The peak shapes were modeled using Thompson–Cox–Hastings pseudo–Voigt function for average grain size and pseudo–Voigt function for weight fraction [53]. Taking the PTA-1-1600 ℃ as an example, the weight fractions of TaC and β-SiC obtained by Rietveld refinement of the XRD patterns are 31.72 wt% and 68.28 wt%, respectively. The average crystallite sizes of 1600 ℃ ceramics derived from AHPCS and Ta-containing single-source-precursors are shown in Fig. 5(b). Compared with the AHPCS-derived ceramic, the grain size of β-SiC increases with the introduction of Ta. The results suggest that in the present study, the crystallization of β-SiC is improved with introduction of Ta. In our previous studies related to SiC/$HfC_xN_{1-x}$/C ceramic nanocomposites, it implies a hindering effect of Hf on the grain growth of β-SiC [38,43]. Our present study with SiC–TaC based nanocomposites obviously exhibits different effects on the crystallization of β-SiC, which should be due to the different molecular structure of single-source-precursor. It is well known that, in PDCs, the grain growth of β-SiC is suppressed by free carbon located on the grain boundary [54]. In this study, $TaCl_5$ was used as precursor for TaC, and therefore no carbon source was introduced. With increasing Ta content, more free carbon was consumed by TaC formation. Therefore, in this study, the sample with higher Ta content exhibits larger grain size of β-SiC due to less free carbon. However, the grain sizes of both β-SiC and TaC are smaller than 31 nm, confirming the formation of SiC–TaC nanocomposites.

To investigate the composition evolution of the ceramics annealed at different temperatures, the chemical compositions of selected ceramics were thus determined by combination of bulk chemical analysis and atomic spectroscopic method, and the results are shown in Table 1. The amorphous ceramic obtained at 900 ℃ has a small amount of hydrogen due to the relatively low annealing temperature. After annealing at 1200 ℃, hydrogen was removed completely and the decomposition of the Si–C–O phase (formed by the reactions of oxygen and moisture adsorbed on the surface of the polymers during the ceramization processe) started, leading to slight decrease of oxygen content from 6.32 wt% to 5.98 wt%. Meanwhile, the phase separation occurred to form crystallites (Fig. 4(a)). At 1400 ℃, the gradual decomposition of the Si–C–O phase accounts for the further decrease of oxygen content. After annealing at 1600 ℃, the oxygen content significantly decreases to 2.27 wt%. In general, the oxygen content is significantly influenced by the annealing temperature while Si, Ta, and C contents slightly change.

TEM was used to investigate the micro/nanostructure evolution of ceramic nanocomposites. The PTA-2 derived ceramics annealed at different temperatures in the range of 1200–1600 ℃ were selected and observed by TEM.

At 1200 ℃, the sample shows a weak crystalline feature in Fig. 6(a), as revealed by the selected area electron diffraction (SAED) pattern. By checking the

**Table 1 Chemical composition of resultant ceramics annealed at different temperatures**

| Sample with different annealing temperature | Chemical composition (wt%) | | | | | Empirical formula |
|---|---|---|---|---|---|---|
| | Si[a] | Ta[b] | C[c] | O[d] | H[e] | |
| PTA-2-900 ℃ | 58.32 | 3.50 | 30.96 | 6.32 | 0.90 | $SiC_{1.243}Ta_{0.009}H_{0.434}O_{0.190}$ |
| PTA-2-1200 ℃ | 58.46 | 3.75 | 31.81 | 5.98 | — | $SiC_{1.274}Ta_{0.010}O_{0.180}$ |
| PTA-2-1400 ℃ | 59.06 | 4.25 | 32.44 | 4.25 | — | $SiC_{1.287}Ta_{0.011}O_{0.126}$ |
| PTA-2-1600 ℃ | 58.01 | 4.50 | 35.22 | 2.27 | — | $SiC_{1.353}Ta_{0.012}O_{0.069}$ |

Note: [a]-determined by the difference; [b]-measured by ICP-S; [c]-measured by carbon/sulfur analyzer; [d]-measured by oxygen/nitrogen analyzer; [e]-measured by elemental analyzer EA/MA1110.

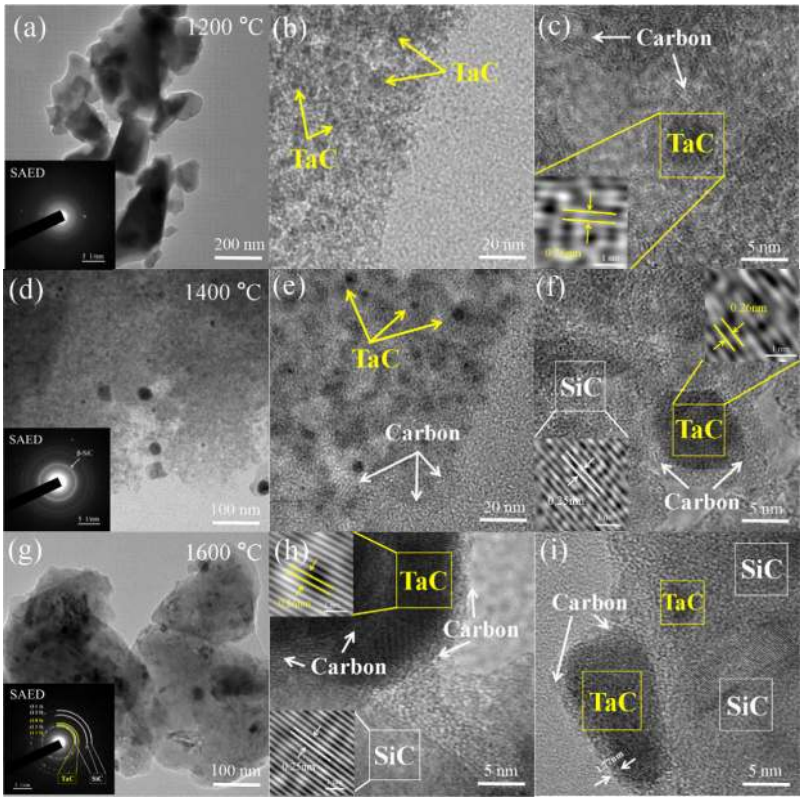


**Fig. 6** (a–c) 1200 ℃ ceramics, (d–f) 1400 ℃ ceramics, and (g–i) 1600 ℃ ceramics. Among all the images, (a, d, g) are bright field images (insets: selected-area electron diffraction), and (b, c, e, f, h, i) are HRTEM images (insets: diffraction patterns obtained by Fourier filtered transformation).

high resolution TEM (HRTEM) images in Figs. 6(b) and 6(c), small TaC crystallites (dark contrast) with a diameter of ca. 5 nm dispersed homogeneously within the matrix. Moreover, turbostratic carbon is observed. After further annealing at 1400 ℃, the SAED pattern clearly indicates the crystallization of β-SiC besides TaC (Fig. 6(d)), which is confirmed by the HRTEM (Figs. 6(e) and 6(f)). Similar to our previous study concerning SiC/$HfC_xN_{1-x}$/C nanocomposites [34], a unique core–shell microstructure is observed for TaC-based nanoparticles. TaC nanoparticles serve as cores and are coated by very thin amorphous carbon, as shown in Fig. 6(f). At 1600 ℃, as shown in Fig. 6(g), β-SiC and TaC crystallites become significantly bigger than the samples annealed at lower temperatures. It is more obvious to observe TaC nanoparticles coated by amorphous carbon layers (Figs. 6(h) and 6(i)). Besides, the TEM images clearly show the phase evolution at 1200 ℃ which cannot be identified by the XRD patterns. The UHTC phase TaC segregated at relative low temperature of 1200 ℃, and then SiC phase started to crystallize at higher temperature of 1400 ℃. The observed microstructure as well as the order of phase segregation agrees well with our previous work related to core–shell structured $HfC_xN_{1-x}$–carbon nanoparticles dispersed in ceramic matrixes [34]. Based on the XRD and TEM results, phase evolution of SiC–TaC–C nanocomposites is demonstrated in Fig. 7.

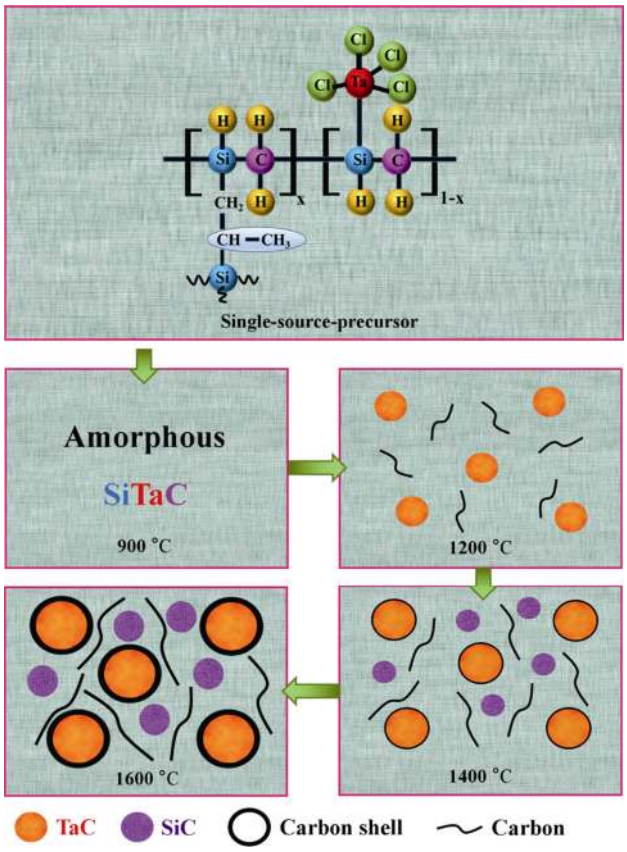


**Fig. 7** Schematic illustration of phase evolution of SiC–TaC–C nanocomposites.

## 4 Conclusions

In conclusion, SiC–TaC–C ceramic nanocomposites were successfully synthesized via a single-source-precursor approach. The UHTC phase TaC segregates after heat treatment at 1200 ℃, and then SiC phase starts to crystallize at higher temperature of 1400 ℃. It is worth mentioning that the TaC phases serve as cores and are coated by very thin amorphous carbon to form core–shell structured TaC@C nanoparticles. Even at high temperature of 1600 ℃, the grain sizes of β-SiC and TaC are on the nanoscale, which confirms the formation of SiC–TaC–C nanocomposites. With the highest amount of $TaCl_5$ in the feed, the weight fractions of TaC and β-SiC obtained by Rietveld refinement of the XRD patterns are 31.72 wt% and 68.28 wt%, respectively. Based on the unique core–shell microstructure, the advanced functional properties of SiC–TaC–C nanocomposites will be further studied in the future.

### Acknowledgements

Zhaoju Yu thanks the National Natural Science Foundation of China (No. 51872246) for financial support.

### References

[1] Ionescu E, Bernard S, Lucas R, *et al*. Polymer-derived ultra-high temperature ceramics (UHTCs) and related materials. *Adv Eng Mater* 2019, **21**: 1900269.

[2] Wu P, Liu SC, Jiang XR. Effect of multi-walled carbon nanotube addition on the microstructures and mechanical properties of Ti(C,N)-based cermets. *J Adv Ceram* 2018, **7**: 58–63.

[3] Xue CQ, Zhou HJ, Hu JB, *et al*. Fabrication and microstructure of $ZrB_2$–ZrC–SiC coatings on C/C composites by reactive melt infiltration using $ZrSi_2$ alloy. *J Adv Ceram* 2018, **7**: 64–71.

[4] Gui KX, Liu FY, Wang G, *et al*. Microstructural evolution and performance of carbon fiber-toughened $ZrB_2$ ceramics with SiC or $ZrSi_2$ additive. *J Adv Ceram* 2018, **7**: 343–351.

[5] Zhang ZF, Sha JJ, Zu YF, *et al*. Fabrication and mechanical properties of self-toughening $ZrB_2$–SiC composites from *in situ* reaction. *J Adv Ceram* 2019, **8**: 527–536.

[6] Nisar A, Ariharan S, Venkateswaran T, *et al*. Oxidation studies on TaC based ultra-high temperature ceramic composites under plasma arc jet exposure. *Corros Sci* 2016, **109**: 50–61.

[7] Fahrenholtz WG, Wuchina EJ, Lee WE, *et al*. *Ultra-high Temperature Ceramics*. Hoboken, NJ, USA: John Wiley & Sons, Inc, 2014.

[8] Liu YZ, Jiang YH, Zhou R, *et al*. First principles study the stability and mechanical properties of MC (M=Ti, V, Zr, Nb, Hf and Ta) compounds. *J Alloys Compd* 2014, **582**: 500–504.

[9] Rezaei F, Kakroudi MG, Shahedifar V, *et al*. Densification, microstructure and mechanical properties of hot pressed tantalum carbide. *Ceram Int* 2017, **43**: 3489–3494.

[10] Chen ZK, Xiong X, Li GD, *et al*. Ablation behaviors of carbon/carbon composites with C–SiC–TaC multi-interlayers. *Appl Surf Sci* 2009, **255**: 9217–9223.

[11] Madhavarao S, Raju CRB, Kumar GSVS. Investigation of friction stir welding of metal matrix composites using a coated tool. *Mater Today: Proc* 2018, **5**: 7735–7742.

[12] Nino A, Hirabara T, Sugiyama S, *et al*. Preparation and characterization of tantalum carbide (TaC) ceramics. *Int J Refract Met Hard Mater* 2015, **52**: 203–208.

[13] Silvestroni L, Pienti L, Guicciardi S, *et al*. Strength and toughness: The challenging case of TaC-based composites. *Compos Part B: Eng* 2015, **72**: 10–20.

[14] Bianchi D, Nasuti F, Onofri M, *et al*. Thermochemical erosion analysis for chraphite/carbon-carbon rocket nozzles. *J Propuls Power* 2011, **27**: 197–205.

[15] Chen LX, Liu ZQ, Shen Q. Enhancing tribological performance by anodizing micro-textured surfaces with nano-$MoS_2$ coatings prepared on aluminum–silicon alloys. *Tribol Int* 2018, **122**: 84–95.

[16] Cui Z, Ke XZ, Li EL, *et al*. Electronic and optical properties of titanium-doped GaN nanowires. *Mater Des* 2016, **96**: 409–415.

[17] Cui Z, Li EL, Ke XZ, *et al*. Adsorption of alkali-metal atoms on GaN nanowires photocathode. *Appl Surf Sci* 2017, **423**: 829–835.

[18] Miller-Oana M, Neff P, Valdez M, *et al*. Oxidation behavior of aerospace materials in high enthalpy flows using an oxyacetylene torch facility. *J Am Ceram Soc* 2015, **98**: 1300–1307.

[19] Khaleghi E, Lin YS, Meyers MA, *et al*. Spark plasma sintering of tantalum carbide. *Scr Mater* 2010, **63**: 577–580.

[20] Liu JX, Kan YM, Zhang GJ. Pressureless sintering of tantalum carbide ceramics without additives. *J Am Ceram Soc* 2010, **93**: 370–373.

[21] Nieto A, Kumar A, Lahiri D, *et al*. Oxidation behavior of graphene nanoplatelet reinforced tantalum carbide composites in high temperature plasma flow. *Carbon* 2014, **67**: 398–408.

[22] Zhang XH, Hilmas GE, Fahrenholtz WG. Densification and mechanical properties of TaC-based ceramics. *Mater Sci Eng: A* 2009, **501**: 37–43.

[23] Talmy IG, Zaykoski JA, Opeka MM. Synthesis, processing and properties of TaC–$TaB_2$–C ceramics. *J Eur Ceram Soc* 2010, **30**: 2253–2263.

[24] Liu H, Liu LM, Ye F, *et al*. Microstructure and mechanical properties of the spark plasma sintered TaC/SiC composites: Effects of sintering temperatures. *J Eur Ceram Soc* 2012, **32**: 3617–3625.

[25] Silvestroni L, Bellosi A, Melandri C, *et al*. Microstructure and properties of HfC and TaC-based ceramics obtained by ultrafine powder. *J Eur Ceram Soc* 2011, **31**: 619–627.

[26] Silvestroni L, Sciti D. Transmission electron microscopy on Hf- and Ta-carbides sintered with $TaSi_2$. *J Eur Ceram Soc* 2011, **31**: 3033–3043.

[27] Pu H, Niu YR, Hu C, *et al*. Ablation of vacuum plasma sprayed TaC-based composite coatings. *Ceram Int* 2015, **41**: 11387–11395.

[28] Niu YR, Pu H, Huang LP, *et al*. Microstructure and ablation property of TaC–SiC composite coatings. *Key Eng Mater* 2016, **697**: 535–538.

[29] Liu LM, Ye F, Zhang ZG, *et al*. Microstructure and mechanical properties of the spark plasma sintered TaC/SiC composites. *Mater Sci Eng: A* 2011, **529**: 479–484.

[30] Eatemadi R, Balak Z. Investigating the effect of SPS parameters on densification and fracture toughness of $ZrB_2$–SiC nanocomposite. *Ceram Int* 2019, **45**: 4763–4770.

[31] Guo SQ. High-temperature mechanical behavior of $ZrB_2$-based composites with micrometer- and nano-sized SiC particles. *J Am Ceram Soc* 2018, **101**: 2707–2711.

[32] Wang LJ, Jiang W, Chen LD. Fabrication and characterization of nano-SiC particles reinforced TiC/SiC nanocomposites. *Mater Lett* 2004, **58**: 1401–1404.

[33] Ionescu E, Kleebe HJ, Riedel R. Silicon-containing polymer-derived ceramic nanocomposites (PDC-NCs): Preparative approaches and properties. *Chem Soc Rev* 2012, **41**: 5032.

[34] Wen QB, Xu YP, Xu BB, *et al*. Single-source-precursor synthesis of dense SiC/$HfC_xN_{1-x}$-based ultrahigh-temperature ceramic nanocomposites. *Nanoscale* 2014, **6**: 13678–13689.

[35] Yuan J, Hapis S, Breitzke H, *et al*. Single-source-precursor synthesis of hafnium-containing ultrahigh-temperature ceramic nanocomposites (UHTC–NCs). *Inorg Chem* 2014, **53**: 10443–10455.

[36] Yuan J, Galetz M, Luan XG, *et al*. High-temperature oxidation behavior of polymer-derived SiHfBCN ceramic nanocomposites. *J Eur Ceram Soc* 2016, **36**: 3021–3028.

[37] Yuan J, Li D, Johanns KE, *et al*. Preparation of dense SiHf(B)CN-based ceramic nanocomposites via rapid spark plasma sintering. *J Eur Ceram Soc* 2017, **37**: 5157–5165.

[38] Wen QB, Feng Y, Yu ZJ, *et al*. Microwave absorption of SiC/$HfC_xN_{1-x}$/C ceramic nanocomposites with $HfC_xN_{1-x}$–

carbon core–shell particles. *J Am Ceram Soc* 2016, **99**: 2655–2663.

[39] Wen QB, Riedel R, Ionescu E. Solid-solution effects on the high-temperature oxidation behavior of polymer-derived (Hf,Ta)C/SiC and (Hf,Ti)C/SiC ceramic nanocomposites. *Adv Eng Mater* 2019, **21**: 1800879.

[40] Wen QB, Riedel R, Ionescu E. Significant improvement of the short-term high-temperature oxidation resistance of dense monolithic HfC/SiC ceramic nanocomposites upon incorporation of Ta. *Corros Sci* 2018, **145**: 191–198.

[41] Wen QB, Yu ZJ, Xu YP, *et al*. SiC/$Hf_yTa_{1-y}CxN_{1-x}$/C ceramic nanocomposites with $HfyTa_{1-y}C_xN_{1-x}$–carbon core–shell nanostructure and the influence of the carbon–shell thickness on electrical properties. *J Mater Chem C* 2018, **6**: 855–864.

[42] Wen QB, Luan XG, Wang L, *et al*. Laser ablation behavior of SiHfC-based ceramics prepared from a single-source precursor: Effects of Hf-incorporation into SiC. *J Eur Ceram Soc* 2019, **39**: 2018–2027.

[43] Wen QB, Yu ZJ, Liu XM, *et al*. Mechanical properties and electromagnetic shielding performance of single-source-precursor synthesized dense monolithic SiC/$HfC_xN_{1-x}$/C ceramic nanocomposites. *J Mater Chem C* 2019, **7**: 10683–10693.

[44] Cai T, Qiu WF, Liu D, *et al*. Synthesis of soluble poly-yne polymers containing zirconium and silicon and corresponding conversion to nanosized ZrC/SiC composite ceramics. *Dalton Trans* 2013, **42**: 4285.

[45] Li YT, Han WJ, Li H, *et al*. Synthesis of nano-crystalline $ZrB_2$/ZrC/SiC ceramics by liquid precursors. *Mater Lett* 2012, **68**: 101–103.

[46] Cheng J, Wang XZ, Wang H, *et al*. Preparation and high-temperature behavior of HfC–SiC nanocomposites derived from a non-oxygen single-source-precursor. *J Am Ceram Soc* 2017, **100**: 5044–5055.

[47] Long X, Shao CW, Wang J, *et al*. Synthesis of soluble and meltable pre-ceramic polymers for Zr-containing ceramic nanocomposites. *Appl Organometal Chem* 2018, **32**: e3942.

[48] Yu ZJ, Lv X, Lai SY, *et al*. ZrC–$ZrB_2$–SiC ceramic nanocomposites derived from a novel single-source precursor with high ceramic yield. *J Adv Ceram* 2019, **8**: 112–120.

[49] Huang TH, Yu ZJ, He XM, *et al*. One-pot synthesis and characterization of a new, branched polycarbosilane bearing allyl groups. *Chin Chem Lett* 2007, **18**: 754–757.

[50] Shriver DF, Drezdzon MA. *The Manipulation of Air-sensitive Compounds*, 2nd edn. New York, USA: John Wiley &Sons Chichester, 1986.

[51] Rodríguez-Carvajal J. Recent advances in magnetic structure determination by neutron powder diffraction. *Phys B: Condens Matter* 1993, **192**: 55–69.

[52] Amorós P, Beltrán D, Guillem C, *et al*. Synthesis and characterization of SiC/MC/C ceramics (M=Ti, Zr, Hf) starting from totally non-oxidic precursors. *Chem Mater* 2002, **14**: 1585–1590.

[53] Li WJ, Li D, Gao X, *et al*. A study on the thermal conversion of scheelite-type $ABO_4$ into perovskite-type $AB(O,N)_3$. *Dalton Trans* 2015, **44**: 8238–8246.

[54] Wen QB, Yu ZJ, Riedel R. The fate and role of *in situ* formed carbon in polymer-derived ceramics. *Prog Mater Sci* 2020, **109**: 100623.